Inorganic Chemistry
Article
Cite This: Inorg. Chem. 2018, 57, 13470−13476
pubs.acs.org/IC

Ground State Nuclear Magnetic Resonance Chemical Shifts Predict Charge-Separated Excited State Lifetimes

Jing Yang,[†] Dominic K. Kersi,[†] Casseday P. Richers,[†] Logan J. Giles,[†] Ranjana Dangi,[†] Benjamin W. Stein,[†] Changjian Feng,[‡] Christopher R. Tichnell,[§] David A. Shultz,*[,§] and Martin L. Kirk*[,†]

[†]Department of Chemistry and Chemical Biology and [‡]College of Pharmacy, The University of New Mexico, Albuquerque, New Mexico 87131-0001, United States

[§]Department of Chemistry, North Carolina State University, Raleigh, North Carolina 27695-8204, United States

Supporting Information

ABSTRACT: Dichalcogenolene platinum(II) diimine complexes, ($L_{E,E'}$)Pt(bpy), are characterized by charge-separated dichalcogenolene donor ($L_{E,E'}$) → diimine acceptor (bpy) ligand-to-ligand charge transfer (LL′CT) excited states that lead to their interesting photophysics and potential use in solar energy conversion applications. Despite the intense interest in these complexes, the chalcogen dependence on the lifetime of the triplet LL′CT excited state remains unexplained. Three new ($L_{E,E'}$)Pt(bpy) complexes with mixed chalcogen donors exhibit decay rates that are dominated by a spin−orbit mediated nonradiative pathway, the magnitude of which is proportional to the anisotropic covalency provided by the mixed-chalcogen donor ligand environment. This anisotropic covalency is dramatically revealed in the ^{13}C NMR chemical shifts of the donor carbons that bear the chalcogens and is further probed by S K-edge XAS. Remarkably, the NMR chemical shift differences also correlate with the spin−orbit matrix element that connects the triplet excited state with the ground state. Consequently, triplet LL′CT excited state lifetimes are proportional to both functions, demonstrating that specific ground state NMR chemical shifts can be used to evaluate spin−orbit coupling contributions to excited state lifetimes.

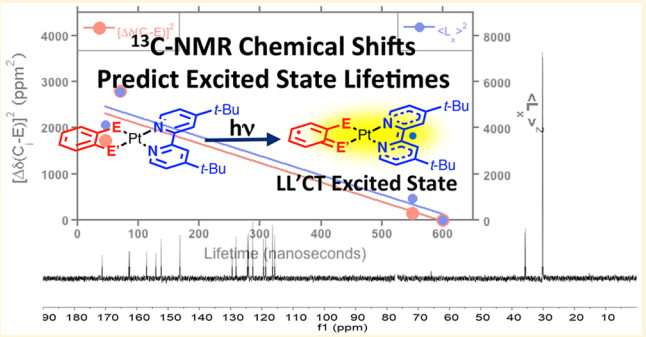

INTRODUCTION

Intersystem crossing (ISC) represents a fundamental nonradiative decay mechanism for relaxation between electronic states of different spin multiplicity.[1−4] As a result of the change in spin state, ISC is an inherently spin-forbidden process.[4] The spin forbiddenness can be overcome via the spin−orbit operator, which mixes states of different spin multiplicity. The ability to obtain molecular-level control over excited states that relax via nonradiative decay channels is central to increasing our ability to harness technologically relevant photoprocesses for the advancement of nanoscale molecule-based photonics,[5−7] optoelectronics,[8−13] solar energy conversion devices,[14−18] photochemical reactivity,[4] and photo-driven molecular motors.[19−21] In marked contrast to radiative triplet → singlet decay (i.e., phosphorescence), which is readily correlated with molecular structure,[4,13] there exists a dearth of structure−property relationships directed toward understanding the mechanism of SOC-promoted ISC. The typical approach for increasing the rate of spin-forbidden nonradiative decay is to employ a heavy atom with a large SOC constant.[4] However, symmetry restrictions can dramatically alter and even eliminate first order out-of-state SOC contributions to electronic relaxation via ISC.[1]

To gain additional insight into the nature of nonradiative T_1 → S_0 ISC, we have synthesized a series of transition metal complexes where the T_1 → S_0 relaxation to the electronic ground state is governed by low-symmetry distortions that derive from the chemical nature of the E/E′ donor atoms in a series of ($L_{E,E'}$)Pt(bpy) ($L_{E,E'}$ = dichalcogenolene, bpy = 4,4′-di-*tert*-butyl-2,2′-bipyridine) complexes (Figure 1). In previous work,[1] we suggested a mechanism to explain why complexes with at least one heavy chalcogen underwent intersystem crossing, while the dioxolene-containing complex (**1-O,O′**) did not. This mechanism involves symmetry-allowed and energetically favorable SO-induced ISC from S_1 → T_2 followed by subsequent relaxation to T_1 for heavy-chalcogen containing complexes, a process that is energetically uphill for **1-O,O′**. The consequence is that **1-O,O′** undergoes rapid radiationless decay from S_1, while the remaining complexes emit weakly from T_1. In the present paper, we explain the chalcogen-

Received: July 24, 2018
Published: October 9, 2018

DOI: 10.1021/acs.inorgchem.8b02087
Inorg. Chem. 2018, 57, 13470−13476

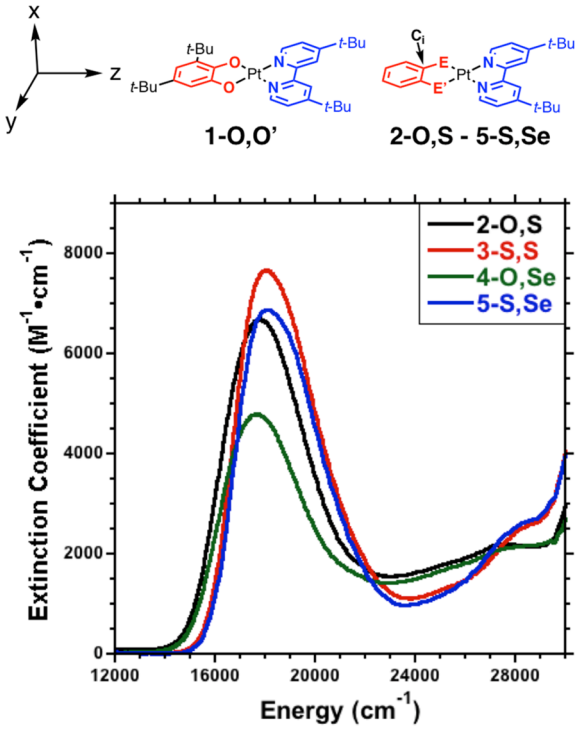

Figure 1. (Top) Structures of $(L_{E,E'})Pt(bpy)$ complexes, **1-O,O′**, **2-O,S**, **3-S,S**, **4-O,Se**, **5-S,Se**, where E,E′ = O,S; S,S; O,Se; S,Se, Pt = +2 oxidation state (d^8), diamagnetic, square-planar transition metal ion, L = dichalcogenolene donor (depicted in red), and bpy = diimine acceptor (depicted in blue). The carbons bearing the chalcogens are labeled C_i. See the Supporting Information for NMR chemical shift assignments. (Bottom) Electronic absorption spectra of $(L_{E,E'})Pt(bpy)$ complexes as solutions in methylene chloride.

dependent lifetimes for the weakly emissive, heavy chalcogen-containing complexes (**2-O,S**−**5-OSe**). Specifically, we present an extraordinary empirical correlation of SOC-induced $T_1 \rightarrow S_0$ nonradiative decay rates with the ^{13}C NMR chemical shift differences between $(L_{E,E'})Pt(bpy)$ dichalcogenolene quaternary carbons, which are labeled as C_i in Figure 1. This provides a unique ground state spectroscopic predictor (NMR) of molecular excited state lifetimes that also directly probes the magnitude of the SOC matrix element that connects the T_1 excited state with the S_0 ground state.

RESULTS AND DISCUSSION

Ligand-Dependent Nonradiative Lifetimes. A distinguishing feature of these chromophores is the presence of a dichalcogenolene → diimine ligand-to-ligand charge transfer (LL′CT) band in the visible region of the spectrum (Figure 1).[22−25] With the exception of **1-O,O′** catecholate complex,[26,27] these complexes display phosphorescent emission with LL′CT excited state lifetimes that are dominated by nonradiative rate constants, which are markedly greater than the radiative rate constants.[1,28] The chromophoric π-systems, **1-O,O′** and **2-S,S**, both possess effective C_{2v} symmetry when neglecting the presence of the *t*-Bu substituents. In the C_{2v} point group, the HOMO and LUMO for **1-O,O′** and **2-S,S** both possess b_1 symmetry. Thus, the ground state term for these complexes is A_1, and this is also the term symbol for the lowest-energy S_1 and T_1 LL′CT excited states.[1] Inspection of Figure 2 indicates that the nature of the chalcogen donor set coordinated to the Pt ion determines whether ISC can occur in

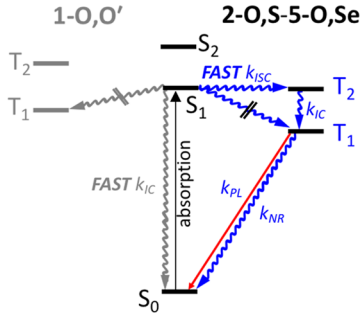

Figure 2. Jablonski diagrams for the observed photoprocesses in **1-O,O′** (left) and the **2-O,S**−**5-S,Se** complexes (right). S_1 and T_1 (arising from the HOMO → LUMO transition) and S_2 and T_2 (arising from the HOMO−1 → LUMO transition) are all LL′CT excited states. Spin−orbit promoted intersystem crossing from S_1 to T_1 is symmetry forbidden, while spin−orbit promoted intersystem crossing from S_1 to T_2 is symmetry allowed. Note that intersystem crossing from S_1 to T_2 in **1-O,O′** does not occur due to the T_2 state lying higher in energy than S_1 for this complex.

the excited state manifold to yield a triplet excited state. When excited state ISC does occur, the nature of the E/E′ donor atoms are observed to control the rate of nonradiative decay to the S_0 electronic ground state. Recently, we compared the relaxation behavior of **1-O,O′**, which is observed to undergo fast, nonradiative relaxation ($\tau_{NR} \approx 650$ ps)[29] from its LL′CT singlet excited state ($^1A_1$, S_1), to complexes that possess heavier chalcogen E/E′ donors and undergo ISC to emissive LL′CT triplet states ($\tau_{T_1} \geq 100$ ns; $\Phi_{em} \approx 0.09$).[1,28] As summarized in Figure 2, the chalcogen dependence on relaxation pathway is a consequence of exergonic, symmetry-allowed SOC-promoted ISC from S_1 to T_2 ($^1A_1 \rightarrow {}^3B_1$), followed by $^3B_1 \rightarrow {}^3A_1$ IC to the T_1 excited state for **2-S,S**.[1] Since the $^1A_1 \rightarrow {}^3B_1$ ISC is energetically uphill[1] for **1-O,O′**, this pathway is unavailable resulting in direct $S_1 \rightarrow S_0$ IC being markedly faster.

Spin−Orbit Coupling Contributions to ISC Rates. A fundamental difference between spin-forbidden ISC and spin-allowed internal conversion (IC) is that the square of the SOC matrix element (i.e., $\langle \varphi_{S_0} | H_{SOC} | \varphi_{T_1} \rangle^2$), which connects the two states of different spin multiplicity, factors into the rate equation for ISC.[30] Under the assumption that all the contributions (e.g., vibronic coupling and Franck−Condon factors) to the rate equation except $\langle \varphi_{S_0} | H_{SOC} | \varphi_{T_1} \rangle^2$ are identical for a series of complexes, the rate of intersystem crossing (k_{NR}) back to the ground state can be expressed as eq 1:[1,4,30]

$$k_{NR} \propto \sum_i \frac{\langle \varphi_{S_0} | \hat{L}_i | \varphi_{T_1} \rangle^2}{(E_{T_1} - E_{S_0})^2} \quad (1)$$

which reduces to eq 2[1,4] when the sum over all indices *x*, *y*, *z* is relegated to only one direction (e.g. *x*).

$$k_{NR} \propto \frac{\langle \varphi_{S_0} | \hat{L}_x | \varphi_{T_1} \rangle^2}{\Delta E^2} \quad (2)$$

The T_1−S_0 energy gaps, ΔE, are essentially the same for the entire series of compounds studied here, indicating that the nonradiative relaxation rate differences across the series do not result from an energy-gap law dependence. For C_{2v} **3-S,S**, there is no spin−orbit matrix element that connects the T_1 ($^3A_1$) and

DOI: 10.1021/acs.inorgchem.8b02087
Inorg. Chem. 2018, 57, 13470−13476

S_0 ($^1A_1$) states. This derives from the fact that there is no $\hat{L}_i$ operator that transforms as a_1 in the C_{2v} point group, resulting in $\langle \varphi_{S_0} | \hat{L}_i | \varphi_{T_1} \rangle = 0$. This spin-forbiddenness results in relatively slow ISC rates for nonradiative relaxation to the electronic ground state.

S K-Edge XAS and Anisotropic Covalency. X-ray absorption spectroscopy at the S K-edge can be used to address Pt−S covalency differences as a function of the mixed dichalcogenolene coordination environment. This is important, since a marked increase in the nonradiative rate constant, k_{NR}, relative to **3-S,S** is observed when two different E,E′ chalcogen donors are coordinated to the Pt^{II} ion in **2-O,S**, **4-O,Se** and **5-S,Se**. This structural perturbation results in an effective molecular symmetry lowering from C_{2v} to C_s. A manifestation of removing the mirror plane and C_2 axis that relates the two S donors in **3-S,S** is that an anisotropic E−Pt−E′ bonding scheme is introduced, with different Pt−E and Pt−E′ bond lengths and covalencies. Coupled with the C_{2v} to C_s lowering of symmetry, the anisotropic Pt−E covalency will permit a rotation of Pt d-orbitals toward the softer E donor atom (Se > S > O) (Figure 3) in the HOMO wave function, which is

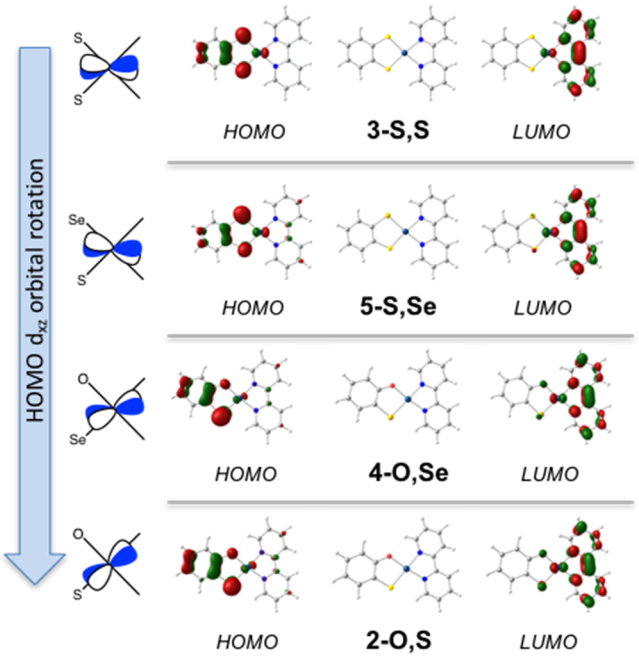

Figure 3. Left: cartoon illustrating d_{xz} orbital rotation in HOMO. Right: Illustration of Kohn−Sham HOMO and LUMO set orbitals. Note d_{xz}-orbital rotation as a function of the chalcogen substitution and that there is no orbital rotation for **3-S,S**.

predominantly Pt-dichalcogenolene in character. Markedly less orbital rotation is expected in the LUMO since it is predominantly Pt-bpy in character.[31] These orbital rotations are important for inducing Pt d-orbital contributions to SOC, which will modify the $T_1 \rightarrow S_0$ decay rates. To address this issue quantitatively, we have collected sulfur K-edge X-ray absorption spectroscopy (XAS) data for **2-O,S**, **3-S,S**, and **5-S,Se** (Figure 4). Sulfur K-edge XAS can quantitate the amount of sulfur p-orbital character present in unoccupied valence molecular orbitals (Figure 3). The sulfur K-edge transitions are sulfur(1s) → sulfur(3p) + Pt(5d) excitations with intensities that are directly proportional to c_i^2, which is the square of the sulfur(3p) atomic orbital coefficient (c_i) in the LCAO (linear combination of atomic orbitals) expansion of the virtual Pt(5d) orbitals:[32,33]

$$\Psi^* = \sqrt{1 - c_i^2}\,\mathrm{Pt(5d)} - c_i \mathrm{S(3p)} \tag{3}$$

Since Pt^{II} is a d^8 ion in a square planar environment, only the Pt d orbital is unoccupied. This in-plane Pt d_{yz} orbital is σ^* antibonding with the chalcogenolene donors, and the sulfur character present in this orbital will reflect the anisotropic covalency[1,34−37] contributions to the E−Pt−E′ bonding scheme in **2-O,S** and **5-S,Se**. This can be directly probed through the intensity of the 1s → ψ^*_{yz} transition at ∼2472 eV. We define the total sulfur 3p orbital character per hole (c_i^2) that contributes to the intensity of the ∼2472 eV 1s → ψ^*_{yz} pre-edge peak according to eq 4:[32,33]

$$D_0 = \frac{h}{3N} c_i^2 I_{s(1s\rightarrow 3p)} \tag{4}$$

where D_0 is the integrated area under this peak, h is the number of holes, N is the number of absorbers, and $I_{s(1s\rightarrow 3p)}$ is the dipole integral for a 1s → 3p transition. We use $I_{s(1s\rightarrow 3p)}$ = 12 for the sulfur donors of the dichalcogenolene ligands[32] in **2-O,S**, **3-S,S**, and **5-S,Se**. This $I_{s(1s\rightarrow 3p)}$ value is based on previously published XAS data that relates the magnitude of the dipole integral with the sulfur 1s → 4p transition energy position.[32] For **3-S,S**, we obtain an experimental value of 22% sulfur character (i.e., 0.22 = c_i^2 per S) admixed into the Pt d_{yz} orbital. This value for c_i^2 is observed to decrease in **5-S,Se** (19.8%), signifying a lesser degree of Pt−S covalency relative to that of Pt−Se covalency. Conversely, c_i^2 is increased in **2-O,S** (22.5%) since the Pt−S bond is more covalent that the Pt−O bond. These trends follow relative electronegativity and chemical hardness[38] values for O, S, and Se and clearly show differences in Pt−E and Pt−E′ bonding for **2-O,S**, **3-S,S** and **5-S,Se**. Although **4-O,Se** does not possess any S atoms and cannot therefore be probed by sulfur K-edge XAS, the observed trends in Figure 3 support an anisotropic bonding scheme for **4-O,Se** as well. We additionally observe a weak shoulder at ∼2471.25 eV that we assign as the 1s → ψ^*_{LUMO} transition. The intensity of the lower-energy 1s → ψ^*_{LUMO} transition is anticipated to be markedly lower than the 1s → ψ^*_{yz} transition, since the LUMO is almost entirely comprised of bpy acceptor ligand character.[1,28] The observed covalency trends also support our anisotropic covalency argument yielding nearly identical S p orbital character in the LUMOs of **3-S,S** and **5-S,Se** (1.4%, 1.6% respectively) and an increase to 2.8% S p orbital character for **2-O,S**.

The results of the S K-edge XAS experiments show anisotropic Pt−E covalency introduced by the difference in the E and E′ donors in **2-O,S**, **4-O,Se**, and **5-S,Se**. This is consistent with the computational results of Figure 3, which show that the Pt d_{xz} orbital component of the dichalcogenolene HOMO rotates toward the softer E donor atom (Se > S > O) (Figure 4).[31] Since the chalcogenide donor atoms are equivalent in **3-S,S**, no Pt d_{xz} orbital rotation is expected. The Pt d orbital rotation observed in the HOMO of **2-O,S**, **4-O,Se**, and **5-S,Se** is in marked contrast to the orientation of the Pt d_{xz} orbital component admixed into the bipyridine LUMO, which should not rotate as much due to the low dichalcogenolene contribution to this orbital and the near chemical equivalence of the bipyridine N donors in this unoccupied LUMO. Thus, the HOMO → LUMO one-electron promotion may be

DOI: 10.1021/acs.inorgchem.8b02087
Inorg. Chem. 2018, 57, 13470−13476

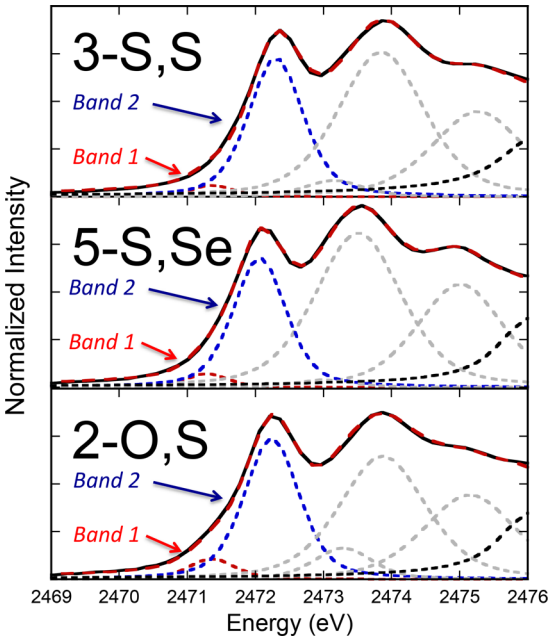

Figure 4. Sulfur K-edge XAS quantifies the degree of anisotropic covalency that is responsible for Pt d-orbital rotation and enhanced $\langle T_1|L_x|S_0\rangle$ SOC. Band 1 (red): 1s → LUMO transition; band 2 (blue): 1s → Pt *yz* transition. The black dashed line is the fit to the rising edge.

described in terms of a Pt d_{xz} orbital rotation upon formation of the S_1 excited state. This orbital rotation results in nonzero $\langle\varphi_{S_0}|\hat{L}_i|\varphi_{T_1}\rangle$ SOC matrix elements, which provides the dominant mechanism for enhanced $T_1 \rightarrow S_0$ nonradiative decay rates in **2-O,S**, **4-O,Se**, and **5-S,Se** relative to **3-S,S**. Complete active-space self-consistent field (CASSCF) calculatations[39] have been utilized to compute the $\langle\varphi_{S_0}|\hat{L}_i|\varphi_{T_1}\rangle$ SOC matrix elements that figure prominently in eq 2. In Figure 5,

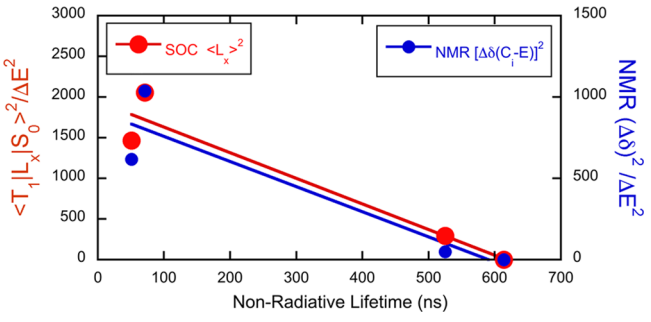

Figure 5. Square of the "ene" quaternary carbon ^{13}C NMR chemical shift difference and square of the SOC matrix element versus ^{3}LL′CT excited state lifetime. Note that the values for the ^{13}C NMR chemical shift difference and square of the SOC matrix element have been divided by the square of the T_1–S_0 energy gap squared according to eq 2.

we plot $\langle\varphi_{S_0}|\hat{L}_i|\varphi_{T_1}\rangle^2/\Delta E^2$ ($\Delta E = E_{T_1} - E_{S_0}$ from emission spectroscopy), which shows the expected increase in the nonradiative $T_1 \rightarrow S_0$ decay that follows the trend predicted from eq 2.

Moreover, the static E–Pt–E′ bond distortions present in **2-O,S**, **4-O,Se**, and **5-S,Se** (e.g., note unequal computed Pt–E and Pt–E′ bond lengths in Figure 4) can be used to understand the nonradiative decay mechanism for **3-S,S**, where $\langle\varphi_{S_0}|\hat{L}_i|\varphi_{T_1}\rangle = 0$. The decreased lifetimes observed for **2-O,S**, **4-O,Se**, and **5-S,Se** all result from an in-plane distortion that closely resembles the in-plane b_2 antisymmetric S–Pt–S stretching vibration in **3-S,S** (C_{2v} symmetry). Dynamic distortions along this vibrational coordinate contribute to a vibronic spin–orbit coupling mechanism that facilitates $T_1 \rightarrow S_0$ relaxation for **3-S,S**. The expression for vibronic spin–orbit coupling is given by eq 5:[2,3]

$$\frac{\partial}{\partial Q}\langle {}^1A_1|\mathcal{H}_{SO}|{}^3A_1\rangle \neq 0 \text{ for } \Gamma_Q = a_2,\ b_1, \text{ and } b_2 \tag{5}$$

where $\mathcal{H}_{SO}$ is the spin–orbit operator, and the Γ_Q are the irreducible representations of the C_{2v} normal modes that promote vibronic spin–orbit coupling. This description of vibronic spin–orbit coupling[3] is similar to Herzberg–Teller coupling,[40] which overcomes the Laporte parity forbiddenness of ligand field transitions in centrosymmetric transition metal complexes through vibronic coupling and also involves odd-parity vibrations of the molecule. Although out-of-plane a_2 and b_1 vibrations will also contribute to this vibronic spin–orbit coupling mechanism, the in-plane b_2 antisymmetric S–Pt–S stretch is clearly a dominant contributor, as shown by our analysis of the static nonradiative decay mechanism observed for **2-O,S**, **4-O,Se**, and **5-S,Se**.

NMR Spectral Probes of Anisotropic Covalency, SOC, and Lifetimes. How then can one "visualize" or consider a common spectroscopic manifestation of ISC that is mediated by out-of-state SOC? Such an observation would allow for a truly unique magneto-structural correlation that would provide keen insight into electronic and geometric structure contributions to nonradiative decay processes. In the present case, the origin of enhanced nonradiative T_1 decay is rooted in dissimilar Pt–E and Pt–E′ bond covalencies that contribute to both static and dynamic modulation of $\langle\varphi_{S_0}|\hat{L}_i|\varphi_{T_1}\rangle$. Although direct spectroscopic probes of the chalcogens themselves are possible, albeit limited (e.g., sulfur K-edge spectroscopy (e.g., sulfur K-edge spectroscopy, Figure 4), the differences in electron densities and electronegativities that result in dissimilar Pt–E and Pt–E′ bond covalencies are conveniently observed and sensitively detected in the different ^{13}C NMR chemical shifts of the quaternary carbon atoms bearing the two different chalcogens $\Delta\delta(C_i\text{–}E)$ in Figure 5; see also Figure 1 and Table 1. This is primarily due to chalcogen electronegativity changes that alter the C_i electron densities,[41] which in turn affect the paramagnetic contributions to the nuclear shielding constants.[42]

Table 1. Excited State Lifetimes, Select ^{13}C NMR Chemical Shifts, and SOC Matrix Elements for ($L_{E,E'}$)Pt(bpy) Complexes[a]

	2-O,S	3-S,S	4-O,Se	5-S,Se
τ_{TA} (ns)	51 ± 10	614 ± 10	71 ± 10	525 ± 10
$\Delta\delta(C_i\text{–}E)$ (ppm)	41.6	0	52.9	12.4
$\langle\varphi_{S_0}\|L_x\|\varphi_{T_1}\rangle$ (cm^{-1})	64	0	74	30
$T_1 \rightarrow S_0$ emission (eV)	1.68	1.77	1.64	1.77

[a]TA = transient absorption; energy units in wavenumbers. See the Supporting Information for TA experimental details and computational details.

DOI: 10.1021/acs.inorgchem.8b02087
Inorg. Chem. 2018, 57, 13470–13476

Remarkably, ground state ^{13}C NMR chemical shift differences allow one to interpret computed $\langle\varphi_{S_0}|\widehat{L}_i|\varphi_{T_1}\rangle$ matrix elements and furthermore predict the effectiveness of excited triplet state nonradiative decay pathways that are promoted by SOC. This result is illustrated graphically in Figure 5, which dramatically shows the relationship between triplet excited state lifetime and (1) the square of the quaternary carbon NMR chemical shift differences $(\Delta\delta(C_i{-}E))^2$ and (2) the square of the CASSCF computed $\langle\varphi_{S_0}|\widehat{L}_x|\varphi_{T_1}\rangle$ SOC matrix elements. The linear relationship between the $T_1 \rightarrow S_0$ lifetime and the square of the SOC matrix element (eq 2) follows from theory.[1,4,30] We note that the experimental data points for $(\Delta\delta(C_i{-}E))^2$ are nearly coincident with those of $\langle\varphi_{S_0}|\widehat{L}_x|\varphi_{T_1}\rangle^2$. This empirical observation indicates that the ^{13}C NMR chemical shifts are accurately reflecting the anisotropic covalency contributions to $\langle\varphi_{S_0}|\widehat{L}_x|\varphi_{T_1}\rangle^2$ and how this matrix element dominates nonradiative decay rate differences in the **2-O,S**−**5-S,Se** series. Thus, differences in C−E,E′ and Pt−E,E′ bonding observed in this series of compounds reflect how the different chalcogen atoms interact with both C and Pt. The differences in C−E,E′ and Pt−E,E bonding are manifest in the chemical shift perturbations on the dichalcogenolene quaternary carbons and anisotoropic covalency in the E−Pt−E′ bonding, respectively. Anisotropic covalency in the E−Pt−E′ bonding scheme is important for inducing critical Pt d orbital rotation differences in the HOMO and LUMO orbitals of this series, leading to predictable $T_1 \rightarrow S_0$ lifetimes that are controlled by SOC.

CONCLUSIONS

We present a rare example of a ground state spectroscopic probe that is both straightforward and easily measured (NMR), which directly correlates with an excited state lifetime that connects states of different spin multiplicity. The three C_s symmetry $(L_{E,E'})Pt(bpy)$ complexes with mixed chalcogen donors, **2-O,S**, **4-O,Se**, and **5-S,Se**, display reduced nonradiative $T_1 \rightarrow S_0$ lifetimes relative to C_{2v} symmetric **3-S,S**. Sulfur K-edge XAS spectroscopy directly shows anisotropic covalency contributions to the E−Pt−E (E = O, S, Se) bonding scheme that is provided by the mixed-chalcogen donor ligand environment. This anisotropic covalency, coupled with $C_{2v} \rightarrow C_s$ symmetry lowering, activates a SOC-mediated nonradiative $T_1 \rightarrow S_0$ ISC relaxation pathway. Here, the decay rate is proportional to the Pt d_{xz} orbital rotation that occurs upon relaxation from the LUMO to the HOMO. Notably, this anisotropic covalency is revealed in the ^{13}C NMR chemical shift differences between the quaternary carbons covalently bound to the chalcogen donors in **2-O,S**, **4-O,Se**, and **5-S,Se**. These C_i−E chemical shift differences are shown to directly correlate with the CASSCF computed spin−orbit matrix element that connects the T_1 excited state with the S_0 ground state, providing an empirical connection between computed out-of-state SOC matrix elements and ground state spectroscopic observables. Since the LL′CT triplet excited state lifetime is observed to increase with the square of both these functions, our results provide an illustrative example of ground state NMR data exposing out-of-state spin−orbit coupling contributions to excited state triplet state lifetimes. These results represent a truly unique excited state magneto-structural correlation, which are expected to apply to other chromophoric systems where metal−ligand anisotropic covalency is important. Further studies associated with this topic are currently underway.

EXPERIMENTAL SECTION

General Experimental. Complexes **2-O,S**, **3-S,S** and **5**−**S-Se** were prepared as described previously.[1] Complex **4-O,Se** was prepared as described in the Supporting Information, page S24, and its triplet excited state lifetime was determined as described previously.[1]

X-ray Absorption Data Collection and Analysis. The S K-edge X-ray absorption spectra of **2-O,S**, **3-S,S**, and **5-S,Se** were collected at the Stanford Synchrotron Radiation Lightsource under standard ring conditions of 3 GeV and ∼500 mA on the unfocused 20-pole 2 T wiggler side-station 4−3, equipped with a liquid N_2 cooled Si(111) double-crystal monochromator for energy selection. All complexes were measured as solids ground directly onto Kapton tape and collected at 90° to the incident beam to avoid fluorescence self-absorption. The beamline was optimized at 2740 eV. $Na_2S_2O_3{\cdot}5H_2O$ was used as calibrant with a maximum pre-edge feature at 2472.02 eV. S K-edge spectra were collected in the energy range of 2420−2740 eV using an unfocused beam in a He-purged fly path at room temperature using a Passivated Implanted Planar Silicon (PIPS) fluorescence detector (CANBERRA). The energy calibration, background correction, data averaging and normalization was accomplished with ATHENA, which is part of the Demeter software package version 0.9.24.[2] The pre-edge features were fitted in Athena using pseudo-Voigt functions and one arctangent step line function for the rising edge. Integration of the pseudo-Voigt functions were performed to define the integrated area of each peak. All parameters of the pseudo-Voigt peaks were allowed to float.

Transient Absorption Lifetime Data. The transient absorption kinetic data were collected using an Edinburgh LP920 laser flash photolysis spectrometer. The excitation source was a Q-switched Continuum Surelite I-10 Nd:YAG laser with a 5 ns pulse width operating at 10 Hz. The excitation pulse was passed through a Continuum Surelite OPO system in order to generate excitation wavelengths in the 400−710 nm range. The pulsed laser source (5 mJ/pulse) was tuned to the maximum absorption wavelength of the sample and focused onto a quartz fluorescence sample cuvette (Starna Cells Inc., path length: 5 mm). Transient absorption and emission spectra were collected using a DH720 ICCD camera mounted on a TMS300 symmetrical Czerny-Turner triple grating monochromator. A Xe lamp was used as the light source for measuring kinetic data at nano- microsecond time scales. The kinetic traces were detected using a red sensitive Hamamatsu R928 photomultiplier covering the 185−870 nm region. Signals from the PMT were recorded on a Tektronix TDS3012C digital storage oscilloscope. All solution data were collected in dichloromethane.

Computational Details. Spin-restricted gas-phase geometry optimizations for all compounds were performed at the density functional level of theory (DFT) by using the Gaussian 09 software package.[31] All the geometry optimizations employed the PBEPBE functional and a def2-TZVP all electron basis set for all the atoms. Using the molecule builder function in the Gaussview 03 software package, the input files were generated. The frontier molecular orbitals were generated for the geometry optimized ground states. The CASSCF method was used to compute reduced spin−orbit coupling matrix elements between lowest triplet states (T_1) and the electronic ground state (S_0). The software program ORCA 4.0[39] was used for the CASSCF computations, where a 4-electron-in-3-orbital (HOMO−1, HOMO, and LUMO) active space was constructed using an all-electron basis set. S K-edge XAS computations were conducted using ORCA (version 3.0.3) on the optimized geometry.[39] The def2-TZVP basis set, B3LYP functional, the zero-order regular approximation (ZORA) were used.

DOI: 10.1021/acs.inorgchem.8b02087
Inorg. Chem. 2018, 57, 13470−13476

■ ASSOCIATED CONTENT

Supporting Information

The Supporting Information is available free of charge on the ACS Publications website at DOI: 10.1021/acs.inorgchem.8b02087.

Synthesis of **4-O,Se**, NMR characterization of all complexes, computational details, and XAS experimental details (PDF)

■ AUTHOR INFORMATION

Corresponding Authors

*E-mail: shultz@ncsu.edu (D.A.S.).
*E-mail: mkirk@unm.edu (M.L.K.).

ORCID

David A. Shultz: 0000-0001-8121-6812
Martin L. Kirk: 0000-0002-1479-3318

Notes

The authors declare no competing financial interest.

■ ACKNOWLEDGMENTS

M.L.K. acknowledges NSF (CHE 1565930 and NSF Grant No. IIA-1301346) for financial support. D.A.S. acknowledges financial support from NSF (CHE-1464085). Use of the Stanford Synchrotron Radiation Lightsource, SLAC National Accelerator Laboratory, is supported by the U.S. Department of Energy, Office of Science, Office of Basic Energy Sciences under Contract No. DE-AC02-76SF00515. The SSRL Structural Molecular Biology Program is supported by the DOE Office of Biological and Environmental Research, and by the National Institutes of Health, National Institute of General Medical Sciences (including P41GM103393). The contents of this publication are solely the responsibility of the authors and do not necessarily represent the official views of NIGMS or NIH.

■ REFERENCES

(1) Yang, J.; Kersi, D. K.; Giles, L. J.; Stein, B. W.; Feng, C. J.; Tichnell, C. R.; Shultz, D. A.; Kirk, M. L. Ligand Control of Donor-Acceptor Excited-State Lifetimes. *Inorg. Chem.* **2014**, *53* (10), 4791−4793.

(2) Rodriguez-Serrano, A.; Rai-Constapel, V.; Daza, M. C.; Doerr, M.; Marian, C. M. Internal heavy atom effects in phenothiazinium dyes: enhancement of intersystem crossing via vibronic spin-orbit coupling. *Phys. Chem. Chem. Phys.* **2015**, *17* (17), 11350−11358.

(3) Tatchen, J.; Gilka, N.; Marian, C. M. Intersystem crossing driven by vibronic spin-orbit coupling: a case study on psoralen. *Phys. Chem. Chem. Phys.* **2007**, *9* (38), 5209−5221.

(4) Turro, N. J.; Ramamurthy, V.; Scaiano, J. *Modern Molecular Photochemistry of Organic Molecules*; University Science Books, 2010.

(5) Saikin, S. K.; Eisfeld, A.; Valleau, S.; Aspuru-Guzik, A. Photonics meets excitonics: natural and artificial molecular aggregates. *Nanophotonics* **2013**, *2* (1), 21−38.

(6) Sutherland, B. R.; Sargent, E. H. Perovskite photonic sources. *Nat. Photonics* **2016**, *10* (5), 295−302.

(7) Green, M. A.; Ho-Baillie, A.; Snaith, H. J. The emergence of perovskite solar cells. *Nat. Photonics* **2014**, *8* (7), 506−514.

(8) Wang, T.; Zhou, C.; Zhang, X. Y.; Xu, D. Waterborne polyurethanes prepared from benzophenone derivatives with delayed fluorescence and room-temperature phosphorescence. *Polym. Chem.* **2018**, *9* (11), 1303−1308.

(9) Wu, H. W.; Zhou, Y. Y.; Yin, L. Y.; Hang, C.; Li, X.; Agren, H.; Yi, T.; Zhang, Q.; Zhu, L. L. Helical Self-Assembly-Induced Singlet-Triplet Emissive Switching in a Mechanically Sensitive System. *J. Am. Chem. Soc.* **2017**, *139* (2), 785−791.

(10) Zhang, J. F.; Xu, X. J.; Yao, C.; Peng, J. H.; Jia, M. P.; Li, L. D. A novel ternary organic microwire radial heterojunction with high photoconductivity. *J. Mater. Chem. C* **2016**, *4* (20), 4505−4511.

(11) Sun, X. X.; Wang, X. J.; Li, X. Y.; Ge, J.; Zhang, Q.; Jiang, J.; Zhang, G. Q. Polymerization-Enhanced Intersystem Crossing: New Strategy to Achieve Long-Lived Excitons. *Macromol. Rapid Commun.* **2015**, *36* (3), 298−303.

(12) Rais, D.; Mensik, M.; Stenclova-Blahova, P.; Svoboda, J.; Vohlidal, J.; Pfleger, J. Time-Resolved Transient Optical Absorption Study of Bis(terpyridyl)oligothiophenes and Their Metallo-Supramolecular Polymers with Zn(II) Ion Couplers. *J. Phys. Chem. A* **2015**, *119* (24), 6203−6214.

(13) Li, E. Y. T.; Jiang, T. Y.; Chi, Y.; Chou, P. T. Semi-quantitative assessment of the intersystem crossing rate: an extension of the El-Sayed rule to the emissive transition metal complexes. *Phys. Chem. Chem. Phys.* **2014**, *16* (47), 26184−26192.

(14) Chang, W.; Congreve, D. N.; Hontz, E.; Bahlke, M. E.; McMahon, D. P.; Reineke, S.; Wu, T. C.; Bulovic, V.; Van Voorhis, T.; Baldo, M. A. Spin-dependent charge transfer state design rules in organic photovoltaics. *Nat. Commun.* **2015**, *6*, 6415.

(15) Guo, F.; Kim, Y.-G.; Reynolds, J. R.; Schanze, K. S. Platinum-acetylide polymer based solar cells: involvement of the triplet state for energy conversion. *Chem. Commun.* **2006**, No. 17, 1887−1889.

(16) Durrant, J. R. Molecular approaches to solar energy conversion: the energetic cost of charge separation from molecular-excited states. *Philos. Trans. R. Soc., A* **2013**, *371* (1996), 20120195.

(17) Gust, D.; Moore, T. A.; Moore, A. L. Solar Fuels via Artificial Photosynthesis. *Acc. Chem. Res.* **2009**, *42* (12), 1890−1898.

(18) Hissler, M.; McGarrah, J. E.; Connick, W. B.; Geiger, D. K.; Cummings, S. D.; Eisenberg, R. Platinum diimine complexes: towards a molecular photochemical device. *Coord. Chem. Rev.* **2000**, *208* (1), 115−137.

(19) Wilcken, R.; Schildhauer, M.; Rott, F.; Huber, L. A.; Guentner, M.; Thumser, S.; Hoffmann, K.; Oesterling, S.; de Vivie-Riedle, R.; Riedle, E.; Dube, H. Complete Mechanism of Hemithioindigo Motor Rotation. *J. Am. Chem. Soc.* **2018**, *140* (15), 5311−5318.

(20) Sawaki, T.; Ishizuka, T.; Kawano, M.; Shiota, Y.; Yoshizawa, K.; Kojima, T. Complete Photochromic Structural Changes in Ruthenium(II)Diimine Complexes, Based on Control of the Excited States by Metalation. *Chem. - Eur. J.* **2013**, *19* (27), 8978−8990.

(21) Cnossen, A.; Hou, L. L.; Pollard, M. M.; Wesenhagen, P. V.; Browne, W. R.; Feringa, B. L. Driving Unidirectional Molecular Rotary Motors with Visible Light by Intra- And Intermolecular Energy Transfer from Palladium Porphyrin. *J. Am. Chem. Soc.* **2012**, *134* (42), 17613−17619.

(22) Bevilacqua, J. M.; Eisenberg, R. Synthesis and Characterization of Luminescent Square-Planar Platinum(II) Complexes Containing Dithiolate or Dithiocarbamate Ligands. *Inorg. Chem.* **1994**, *33*, 2913−2923.

(23) Cummings, S. D.; Eisenberg, R. Tuning the Excited-State Properties of Platinum(II) Diimine Dithiolate Complexes. *J. Am. Chem. Soc.* **1996**, *118*, 1949−1960.

(24) Paw, W.; Cummings, S. D.; Mansour, M. A.; Connick, W. B.; Geiger, D. K.; Eisenberg, R. Luminescent Platinum Complexes: Tuning and Using the Excited State. *Coord. Chem. Rev.* **1998**, *171*, 125−150.

(25) Zuleta, J. A.; Bevilacqua, J. M.; Eisenberg, R. Solvatachromic and Emissive Properties of Pt(II) Complexes with 1,1- and 1,2-Dithiolates. *Coord. Chem. Rev.* **1991**, *111*, 237−248.

(26) Kamath, S. S.; Uma, V.; Srivastava, T. S. Neutral mixed-ligand complexes of platinum(II) and palladium(II) with α-diimine and dioxolenes. *Inorg. Chim. Acta* **1989**, *166* (1), 91−98.

(27) Scattergood, P. A.; Jesus, P.; Adams, H.; Delor, M.; Sazanovich, I. V.; Burrows, H. D.; Serpa, C.; Weinstein, J. A. Exploring excited states of Pt(II) diimine catecholates for photoinduced charge separation. *Dalt. Trans.* **2015**, *44*, 11705−11716.

(28) Cummings, S. D.; Eisenberg, R. Luminescence and Photochemistry of Metal Dithiolene Complexes. *Prog. Inorg. Chem.* **2004**, *52*, 315−367.

DOI: 10.1021/acs.inorgchem.8b02087
Inorg. Chem. 2018, 57, 13470−13476

(29) Best, J.; Sazanovich, I. V.; Adams, H.; Bennett, R. D.; Davies, E. S.; Meijer, A.; Towrie, M.; Tikhomirov, S. A.; Bouganov, O. V.; Ward, M. D.; Weinstein, J. A. Structure and Ultrafast Dynamics of the Charge-Transfer Excited State and Redox Activity of the Ground State of Mono- and Binuclear Platinum(II) Diimine Catecholate and Bis-catecholate Complexes: A Transient Absorption, TRIR, DFT, and Electrochemical Study. *Inorg. Chem.* **2010**, *49* (21), 10041−10056.
(30) Simons, J. *Energetic Principles of Chemical Reactions*; Jones and Bartlett: Boston, MA, 1983.
(31) Frisch, M. J.; Trucks, G. W.; Schlegel, H. B.; Scuseria, G. E.; Robb, M. A.; Cheeseman, J. R.; Scalmani, G.; Barone, V.; Mennucci, B.; Petersson, G. A.; Nakatsuji, H.; Caricato, M.; Li, X.; Hratchian, H. P.; Izmaylov, A. F.; Bloino, J.; Zheng, G.; Sonnenberg, J. L.; Hada, M.; Ehara, M.; Toyota, K.; Fukuda, R.; Hasegawa, J.; Ishida, M.; Nakajima, T.; Honda, Y.; Kitao, O.; Nakai, H.; Vreven, T.; Montgomery, J. A., Jr.; Peralta, J. E.; Ogliaro, F.; Bearpark, M.; Heyd, J. J.; Brothers, E.; Kudin, K. N.; Staroverov, V. N.; Kobayashi, R.; Normand, J.; Raghavachari, K.; Rendell, A.; Burant, J. C.; Iyengar, S. S.; Tomasi, J.; Cossi, M.; Rega, N.; Millam, J. M.; Klene, M.; Knox, J. E.; Cross, J. B.; Bakken, V.; Adamo, C.; Jaramillo, J.; Gomperts, R.; Stratmann, R. E.; Yazyev, O.; Austin, A. J.; Cammi, R.; Pomelli, C.; Ochterski, J. W.; Martin, R. L.; Morokuma, K.; Zakrzewski, V. G.; Voth, G. A.; Salvador, P.; Dannenberg, J. J.; Dapprich, S.; Daniels, A. D.; Farkas, O.; Foresman, J. B.; Ortiz, J. V.; Cioslowski, J.; Fox, D. J. *Gaussian 09*, revision E.01; Gaussian, Inc.: Wallingford, CT, 2009.
(32) Sarangi, R.; DeBeer George, S.; Rudd, D. J.; Szilagyi, R. K.; Ribas, X.; Rovira, C.; Almeida, M.; Hodgson, K. O.; Hedman, B.; Solomon, E. I. Sulfur K-edge X-ray absorption spectroscopy as a probe of ligand-metal bond covalency: Metal vs ligand oxidation in copper and nickel dithiolene complexes. *J. Am. Chem. Soc.* **2007**, *129* (8), 2316−2326.
(33) Szilagyi, R. K.; Lim, B. S.; Glaser, T.; Holm, R. H.; Hedman, B.; Hodgson, K. O.; Solomon, E. I. Description of the ground state wave functions of Ni dithiolenes using sulfur K-edge X-ray absorption spectroscopy. *J. Am. Chem. Soc.* **2003**, *125* (30), 9158−9169.
(34) DeBeer George, S.; Metz, M.; Szilagyi, R. K.; Wang, H. X.; Cramer, S. P.; Lu, Y.; Tolman, W. B.; Hedman, B.; Hodgson, K. O.; Solomon, E. I. A quantitative description of the ground-state wave function of Cu-A by X-ray absorption spectroscopy: Comparison to plastocyanin and relevance to electron transfer. *J. Am. Chem. Soc.* **2001**, *123* (24), 5757−5767.
(35) Helton, M.; Gruhn, N.; McNaughton, R.; Kirk, M. Control of oxo-molybdenum reduction and ionization potentials by dithiolate donors. *Inorg. Chem.* **2000**, *39* (11), 2273−2278.
(36) Izumi, Y.; Glaser, T.; Rose, K.; McMaster, J.; Basu, P.; Enemark, J. H.; Hedman, B.; Hodgson, K. O.; Solomon, E. I. Ligand K-Edge and Metal L-Edge X-Ray Absorption Spectroscopy and Density Functional Calculations of Oxomolybdenum Complexes with Thiolate and Related Ligands: Implications for Sulfite Oxidase. *J. Am. Chem. Soc.* **1999**, *121* (43), 10035−10046.
(37) Helton, M. E.; Kirk, M. L. A model for ferricyanide-inhibited sulfite oxidase. *Inorg. Chem.* **1999**, *38* (20), 4384−4385.
(38) Parr, R. G.; Pearson, R. G. Absolute Hardness - Companion Parameter to Absolute Electronegativity. *J. Am. Chem. Soc.* **1983**, *105* (26), 7512−7516.
(39) Neese, F. The ORCA program system. *Wiley Interdisciplinary Reviews: Computational Molecular Science* **2012**, *2* (1), 73−78.
(40) Solomon, E. I. Inorganic Spectroscopy, An Overview. In *Comm. Inorg. Chem.*; Sutin, N., Ed.; Gordon and Breach: New York, 1984; Vol. *3*.
(41) Olah, G. A.; Mateescu, G. D. Stable carbonium ions. CI. Tetraphenylcyclobutadiene dication. *J. Am. Chem. Soc.* **1970**, *92* (5), 1430−1432.
(42) Karplus, M.; Pople, J. A. Theory of Carbon NMR Chemical Shifts in Conjugated Molecules. *J. Chem. Phys.* **1963**, *38* (12), 2803−2807.

DOI: 10.1021/acs.inorgchem.8b02087
Inorg. Chem. 2018, 57, 13470−13476